JACS
JOURNAL OF THE AMERICAN CHEMICAL SOCIETY

ARTICLE

pubs.acs.org/JACS

Size and Shape Dependence of the Photocatalytic Activity of TiO_2 Nanocrystals: A Total Scattering Debye Function Study.

Giuseppe Cernuto,[†,‡] Norberto Masciocchi,[†] Antonio Cervellino,[§] Gian Maria Colonna,[‡] and Antonietta Guagliardi*[,†,⊥]

[†]Dipartimento di Scienze Chimiche e Ambientali, Università dell'Insubria, via Valleggio 11, 22100 Como, Italy

[‡]Stazione Sperimentale per la Seta, via Valleggio 3, 22100 Como, Italy

[§]SLS, Paul Scherrer Institut, 5232 Villigen PSI, Switzerland

[⊥]Istituto di Crystallografia, CNR, via Amendola 122/O, 70126 Bari, Italy

Supporting Information

ABSTRACT: Nanocrystalline TiO_2 samples, prepared for smart textiles applications by the sol−gel technique in acidic or basic media, have been characterized by synchrotron X-ray powder diffraction and total scattering methods based on a fast implementation of the Debye function and original algorithms for sampling interatomic distances. Compared to the popular and widely used Rietveld-based approaches, our method is able to simultaneously model both Bragg and diffuse contributions and to quantitatively extract either sizes and size distribution information from the experimental data. The photocatalytic activity of the investigated samples is here systematically correlated to the average sizes and size distributions of anisotropically shaped coherent domains, modeled according to bivariate populations of nanocrystals grown along two normal directions.

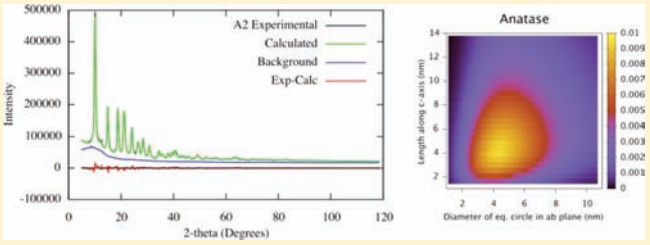

INTRODUCTION

Titanium dioxide nanoparticles have attracted the interest of many chemists[1] who, in the vigorous attempt to characterize, tune, and exploit their excellent photochemical activity, have employed a wide range of synthetic approaches, experimental, analytical, and structural methods as well as sophisticated computational and modeling techniques.[2] Despite the tremendous amount of work put into these systems, the complete understanding of this (apparently simple) material and of its structure−property relationship seems not to be fully achieved. In particular, many papers have been aimed at clarifying the dependence of the functional properties on the occurring polymorphs (anatase, rutile, and brookite[3]) or on a mixture thereof, on the particle size and shape, on the structural defects, etc.

In this field, commonly applied (micro)structural characterization techniques are TEM/HRTEM, often used to get information about the particles' shape and aspect ratio, and wide-angle X-ray diffraction methods, mainly used to provide volume-averaged isotropic size estimations and qualitative shape information. However, since the intrinsic *structural* and *morphological* anisotropy of nanocrystalline TiO_2 seems to deeply affect the local stereochemistry of the surface atoms,[4] the development of defects[5−7] and, finally, the optical band gap value[8] and the efficiency of charge separation and migration,[9] a more exhaustive morphological characterization of this system is required, in a more detailed (statistically meaningful) approach. Nevertheless, particles' sizes and shapes and their distributions, all featuring real samples, have rarely[7,10] been simultaneously and quantitatively determined along with structure types and concentrations (through one or both aforementioned techniques) to systematically account for the photocatalytic properties of a family of TiO_2 specimens showing size and shape evolution. Limitations on such an issue arise from the local nature of TEM techniques, making them a pretty weak statistical probe, while the simple approximations inherent in the widely used powder diffraction Rietveld-like approach (e.g., crystal size peak-broadening[11]) are able to give only average isotropic size values without any detail on size and shape dispersions. Furthermore, such a phenomenological approach tends to fail when the nanocrystal sizes are of a few nm and diffraction traces show either Bragg and diffuse scattering contributions. Total scattering methods (namely, pair distribution function − PDF[12] and Debye function analysis − DFA[13]) are, in this case, to be preferred, since they are able to model both effects.

In particular, the DFA method[14] describes the scattered intensity from orientationally isotropic systems (gases, liquids, and random powders) through the simple, but extremely time-consuming, formula:[15]

$$I(q) = \sum_i \sum_j f_i f_j \sin(qr_{ij})/(qr_{ij})$$

Received: November 14, 2010
Published: February 16, 2011

(where i,j run on all atoms, $q = 4\pi(\sin\theta)/\lambda$, r_{ij}, are the interatomic distances, and f_k the atomic form factors). However, the development of suitable algorithms for distance sampling[16] and pattern modeling has recently turned the Debye formula into an efficient and powerful computational tool and made it possible to employ this technique in the characterization of metallic[17] or ionic nanocrystals,[18] as well as of more complex inorganic biomaterials.[19]

In this paper we present a DFA study to quantitatively characterize a number of TiO_2 samples containing very small anisotropically shaped nanocrystals (NCs, with average sizes below 10 nm) and to correlate the photocatalytic activity with the average size and NCs aspect ratio.

Most of the TiO_2-based materials have been studied for addressing photocatalytic activity in water-splitting reactions, pollutant decomposition, and solar-energy capture. Our specific interest in titania nanoparticles deals with the appealing goal of tailoring suitable coatings for smart textiles, in which stains and odors can be removed by exposure to solar light.[20] Sizes in the regime of a few nanometers and formed at low temperatures, enabling an evenly distributed deposition on fibers and yarns, are necessary to allow the growth and the accommodation of the nanocrystals on the surface of the threads.

EXPERIMENTAL SECTION

Synthesis of TiO_2 Nanocrystals. Titania nanoparticles were prepared by the sol−gel route, employing different conditions for the A and C (acidic) samples and for the B (basic) samples; during all our preparations (vide infra) the temperature was kept low enough to grant the formation of very small (still active) materials. Heat treatment (calcination), increasing crystal size, crystal perfection, and photocatalytic activity were therefore deliberately avoided.

A Samples. To a 1.4 M HCl solution in water/ethanol was added titanium tetraisopropoxide (TTIP) dropwise under stirring. Molar ratio employed: TTIP/$H_2O_{(HCl)}$/EtOH = 1:25:15. The obtained colloidal suspension was then kept under vigorous stirring for 24 h at rt, then divided into three portions, aged for 24 h in an oven at rt, 45, and 80 °C (samples A0, A1, and A2, respectively). During this time A1 and A2 turned into a white gel (A0 remaining practically unchanged). A1 and A2 were then completely dried (at 45 and 80 °C, respectively), forming white, solid xerogels, later ground into fine powders.

AHW (Hot Water) Sample. A colloidal suspension, prepared as described above for the A samples, has been refluxed for 2 h, and was then dried in an oven at 80 °C.

B Samples. To a NaOH solution in water/ethanol (pH 9.00) was added TTIP dropwise under stirring. Molar ratio employed: TTIP/$H_2O_{(pH\ 9.00)}$/EtOH = 1:25:15. The obtained suspension was then kept under vigorous stirring for 24 h at rt, then divided into three portions (containing amorphous particles, XRD evidence) aged in an oven at 80 °C for 24, 48, and 120 h (samples B1, B2, and B3, respectively). The solids were then separated by centrifugation, repeatedly washed with distilled water, and dried.

C Samples. To a 3 M CH_3COOH solution in water/ethanol was added TTIP dropwise under stirring. Molar ratio employed: TTIP/$H_2O_{CH_3COOH}$/EtOH = 1:325:15. The obtained colloidal suspension was then kept under vigorous stirring for 24 h at rt, then divided into two portions, and aged in an oven at 80 °C for 24 and 120 h (samples C1 and C2, respectively).

Characterization. The photocatalytic activity of our samples has been evaluated by suspending 25 mg of TiO_2 in an aqueous solution (35 mL) of methylene blue (MB, 15 mg/L) in a Petri capsule. Irradiation by a 300-W solar lamp OSRAM UltraVitalux[21] set vertically 50 cm apart allowed complete decoloration within a few hours. The MB concentration was evaluated spectrophotometrically (λ_{max} = 667 nm). Each test was repeated four times, obtaining nearly coincident [MB] values with the apparent kinetic constants (k, in a pseudo-first-order approximation) collected in Table 1.

Table 1. Relevant Analytical and Microstructural Parameters for Anatase, Derived from the DFA Analysis of the A1, A2, AHW, B1, B2, B3, C1, and C2 Titania-Based Materials[a]

sample	χ	D_{ab}	L_c	D_{eq}	L_c/D_{ab}	k, min^{-1}	occ (Ti)
A1	0.68	4.0	3.8	4.4	0.95	0.0152	0.90
A2	0.80	5.6	6.7	6.6	1.18	0.0223	0.93
AHW	0.74	4.2	4.1	4.6	0.98	0.0184	0.91
B1	0.73	5.9	6.7	6.7	1.14	0.0109	0.94
B2	0.78	6.0	6.8	6.9	1.14	0.0080	0.95
B3	0.78	6.2	6.8	7.1	1.10	0.0050	0.96
C1	1.00	6.1	11.9	8.4	2.08	0.0017	0.90
C2	1.00	6.6	13.9	9.3	2.13	0.0012	0.91

[a] D_{ab}, L_c, and D_{eq} (defined in the text) are in nanometers and are based on the NCs *mass* distribution.

High-quality synchrotron X-ray powder diffraction data (ensuring high counting statistics without significant instrumental contribution to peak broadening) were collected at rt at the high resolution Material Science Beamline at SLS, Paul Scherrer Institut, using a 0.3 mm glass capillary and 0.620639 Å radiation (calibrated with the NIST standard 640b silicon powder). Independent measurements of the empty glass capillary and air scattering contributions were performed and used in the analysis.

The Total Scattering Debye Function Method. The method used to characterize the titania nanoparticles is a Total Scattering approach based on a new and fast implementation of the Debye equation, coupled to a physically sound atomistic model of a bivariate population of TiO_2 nanoclusters. The Debye formula[15] is known since 1915 and takes the advantage of simultaneously modeling Bragg and diffuse scattering, both collected from a short-range ordered material such as a nanocrystalline powder, as a function of the distribution of interatomic distances within the sample. However, in its original formulation, the Debye equation is extremely expensive from the computational point of view, as the number of interatomic distances increases with the square and with up to the sixth power of the nanocrystal linear size, for ordered and disordered materials, respectively.

Briefly, our innovative strategy to DFA relies on three basic choices:

(i) A bottom-up approach aiming at generating a population of atomistic nanocrystal (NC) models of increasing size and suitable shapes. Anisotropic (rod- and platelike) shapes are built through a layer-by-layer construction and under the assumption, holding for biaxial systems, of two distinct "growth" modes, one along the highest-order symmetry crystallographic axis and the second one in the orthogonal plane. This step is speeded up by combining the Patterson vectors and the unit cell lattice vector translations.

(ii) The use of sampled interatomic distances,[16b] instead of the original ones, reducing the number of terms in the Debye equation by orders of magnitude (growing as the *linear* NC size), without losing accuracy in the pattern calculation. The sampled distances of each nanocrystal are stored in suitable databases to be used in the subsequent DFA process.

(iii) A modified Debye formula[16b] that, thanks to the constant step used for encoding the sampled distances, takes advantage of the recursive properties of Chebyshev polynomials of the second kind and makes the calculations fast enough to deal with the

pattern of hundreds of nanocrystals and to use iterative global optimization algorithms.

Furthermore, a number of adjustable parameters are involved in the pattern model. To account for size and shape distributions of a population of nanocrystals of different sizes and shapes, a bivariate log-normal function[22] is adopted, and five parameters are used to describe the average/standard deviation pairs of the size distributions along the two growth directions and their correlation angle (details given in Supporting Information [SI]). Possible lattice expansions/contractions as a function of crystal size are also dealt with. Among the structural parameters, the adjustable ones are atomic site occupancy factors and (up to) three coefficients that linearly correct the isotropic atomic Debye−Waller factor as a function of size.

For the titania samples here investigated, a bivariate population of prismatic nanocrystals were generated for the two detected polymorphs (anatase and brookite, vide infra). Reasons for such a choice are given in the Results and Discussion section. About 40 min was necessary to create all the required sampled distances databases on a Mac OS X 10.6.4 machine using a 3.2 GHz Intel Core i3 processor. The DFA study was performed using the recently published DEBUSSY suite of programs.[23]

RESULTS AND DISCUSSION

All TiO_2 samples show the evident trace of nanocrystalline anatase and, in the A- and B-type samples, a (apparently) small amount of brookite, as already evidenced by others in analogous preparations.[7] The bivariate sets of atomistic clusters of increasing size were created with sizes up 15 nm in the *ab*-plane and 30 nm along the *c*-axis, for anatase, and up to 6 and 10 nm in *ab* and along *c*, respectively, for brookite. Of course, each real nanocrystal in our samples has its own shape, which we assumed to be approximated by a simple square prism. Such a choice is justified by two main reasons: first, by crystal symmetry. For anatase (space group $I4_1/amd$), in agreement with the recent report[24] on shapes found in its nanocrystals (different from the bipyramidal morphology of macroscopic crystals), the chosen polyhedron might not be very far from reality. For brookite (space group *Pbca*), we permuted the axes of the ICSD entry 36408, in order to have **c** as the longest axis and **a** and **b** of nearly equal lengths. Accordingly, the latter axes, symmetry unrelated, are treated by a common growth parameter, to match the bivariate size distribution model discussed above; this is clearly an approximation, partially justified by the very small size of brookite NCs and by its low molar content in the samples (if present). The second motivation for the choice of prismatic crystals derives from the fact that the fine details of the NC shapes are not very important from the point of view of wide-angle powder diffraction, *as long as the principal axes of the base remain comparable.* Consequently, the level of shape information which can reliably be extracted—as a statistical distribution—is the *prism aspect ratio*, while higher-level shape details are likely lost in the experimental trace, either intrinsically or because of being averaged out.

Two distinct sampled distances databases, referring to slightly different anatase cell parameters, were necessary for modeling data of the (A1, A2, AHW, C1, C2) and (B1, B2, B3) groups (vide infra), while only one sampled distance database was built for brookite. Apparently, as also checked by a conventional Rietveld refinement approach coupled to a spherical harmonics description of the anisotropic peak broadening, lattice parameters of anatase depend more significantly on the synthetic method (acidic in the A, C samples, or basic in the B preparations) than on the size/shape properties derived from our DFA. Matching of the total scattering pattern models with experimental data was optimized[25] by refining, for each phase, the parameters of the bivariate log-normal size distribution, Ti site occupancy factor and additional size-dependent (apparent) Debye−Waller factors. Allowance for a size-dependent interatomic distances deformation resulted not to be necessary and the variation of (average) lattice parameters for all NCs within the same family turned out to be negligibly small. The best fit, for specimen A2, is shown in Figure 1 along with the population distribution of anatase and brookite crystal sizes derived therefrom. Analogous plots for the other samples are collected in the SI. Worth noting in the anatase 2D maps is the quite large size spread around the average values in both the growth directions and the small correlations between the two, nearly vanishing for the B-type samples.[26]

The most relevant findings of this analysis are summarized in Table 1 and in Figures 2 and 3. The weight percent (equivalent, for polymorphic phases, to the molar fraction χ) of brookite (where present) was estimated to lie in the 20−32% range. These values were used to normalize the sample photocatalytic activity (k) by assuming anatase as the only active polymorph. This is a clear approximation, since brookite nanocrystals have occasionally shown significant photocatalytic activity;[27] however, had renormalization of the k values on the anatase content not been considered, our results would equally hold.

All average sizes (the diameter of the equivalent circle in the *ab*-plane, D_{ab}, the domain length along the *c*-axis, L_c, and the diameter of the equivalent sphere, D_{eq}), in nanometers, and their distributions (see the complete Tables in SI) are derived from the NCs *mass distribution*.[28] *Number distribution*-based values, systematically smaller than the former ones, are also supplied in the SI.

Independently of the average values, all samples are relatively polydispersed (see Figure 1 and SI). Therefore, the comparison of the two types of (*mass*- and *number*-based) statistics enabled us to detect possible differences between the smallest- and the largest-sized fractions within each sample.

Different aging times (under isothermal conditions) of the B1, B2, B3 and C1, C2 samples slightly increase the sizes of anatase (in both directions, see Figure 2) and induce a higher aspect ratio L_c/D_{ab}[29] at the smallest sizes (see SI) and a near constancy for the largest NCs. Differently, for brookite (not occurring in C1 and C2), the two sizes show opposite trends. Larger sizes are also found for anatase on increasing temperature in the A1 and A2 samples, with a relevant difference of the aspect ratios derived from the mass and number distributions of A1.[30] Sample AHW, refluxed in hot water for only 2 h, shows a moderate increase of L_c and D_{ab} crystal sizes (if compared to A2, aged at 80 °C for 24 h) and a mass-based aspect ratio very similar to that of A1. The use of a different acid (CH_3COOH vs HCl) induces in the C1 and C2 samples larger particles with a significantly increased morphological anisotropy, with aspect ratios well above 2.

To compare the photochemical activity of all the samples, the kinetic constants derived from methylene blue discoloration under isothermal conditions are shown in Figure 3 as a function of the average diameter of the equivalent sphere (D_{eq}). A clear trend of k, lowering at increasing size, can be observed, with the notable exception of A1 and AHW, the samples with the smallest crystal sizes. Looking at Table 1, these samples also appear to possess the smallest (*mass*-derived) aspect ratios.

Such finding seems to confirm that both size and shape affect the photochemical activity, as if the electron transfer to MB was different on distinct NCs facets, within a rather complex interplay

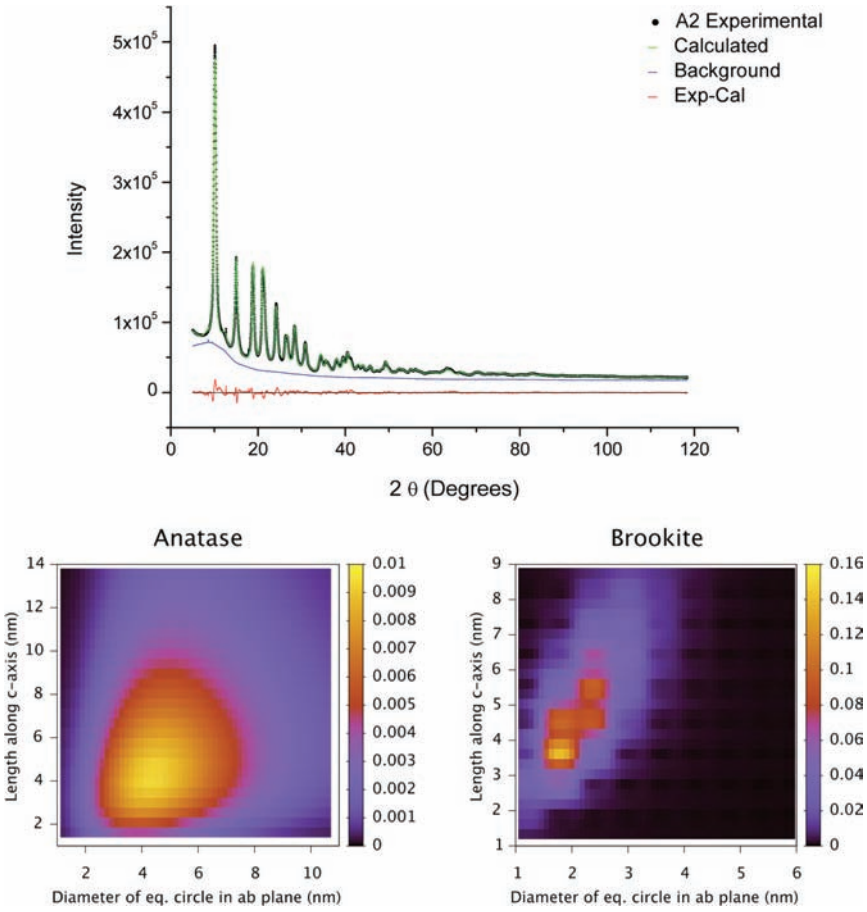

Figure 1. (Top) Final best fit for specimen A2, obtained by the DFA approach. Black: synchrotron X-ray diffraction data; green: simulated pattern; blue: background trace; red: difference plot. (Bottom) Two-dimensional maps of the bivariate size distributions for anatase (left) and brookite (right) in the *ab*-plane (D_{ab}, horizontal axes, nm) and the *c*-axis (L_c, vertical axes, nm). Note the difference in the *xy* scales in the two plots. Two-dimensional graphics drawn with *Gnuplot* (Williams, T.; Kelley, C. 2007, http://www.gnuplot.info).

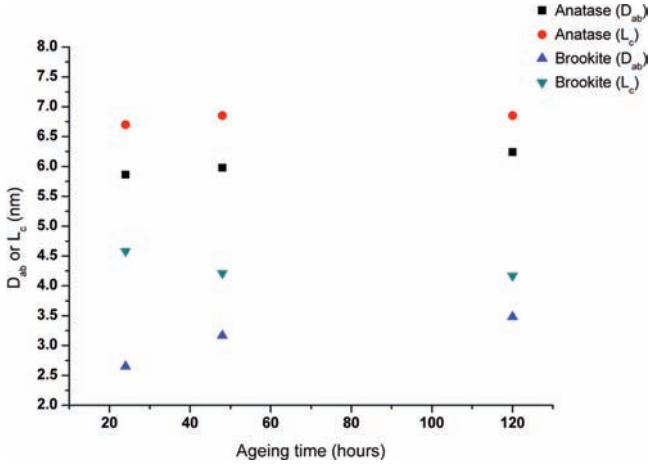

Figure 2. Average sizes in the *ab*-plane and along the *c*-axis (D_{ab} and L_c in nm, for anatase and brookite components) of the B1, B2, and B3 samples vs aging time.

among facets extension and surface/volume atomic ratio. However, the paucity of titania nanocrystals possessing D_{eq} values intermediate between (A1, AHW) and A2 with markedly different aspect ratios does not allow us to assess the robustness of the latter statement. Significantly, the clear trend retrieved for the remaining six samples strengthens the power of the method in quantitatively rescuing small microstructural differences from apparently similar powder diffraction traces.

Further important structural details found by DFA (see SI) appear partially consistent with the most recent reports. In fact, progressively increasing cell volumes are reported for the smaller anatase NCs when sizes are less than 10 nm,[7] independently of the synthesis route. Our analysis registers a moderate cell expansion for the acidic synthesis samples (V = 136.7 Å^3 for A1, A2, AHW, C1, C2), when compared to those prepared in basic conditions (V = 135.3 Å^3 for B1, B2, B3). As anticipated, lattice parameters depend more significantly on the synthetic method than on the size/shape properties derived from our DFA, the previously reported trend not being observed in the A- and C-type samples, which span a wide range of D_{eq} values below 10 nm.

The (average) site occupancy factor of Ti in the anatase nanocrystals falls in the narrow 0.90−0.96 range. Interestingly, separate clustering of the significantly lower values are observed for the A and C samples (possibly due to H^+ incorporation) and of the larger values for the B ones. The occurrence of metal ion vacancies in sol−gel prepared titania nanoparticles is also quoted in previous reports, with a decrease of Ti vacancies with larger average particle sizes,[5,7] the missing titanium ions likely being

dx.doi.org/10.1021/ja110225n |*J. Am. Chem. Soc.* 2011, 133, 3114–3119

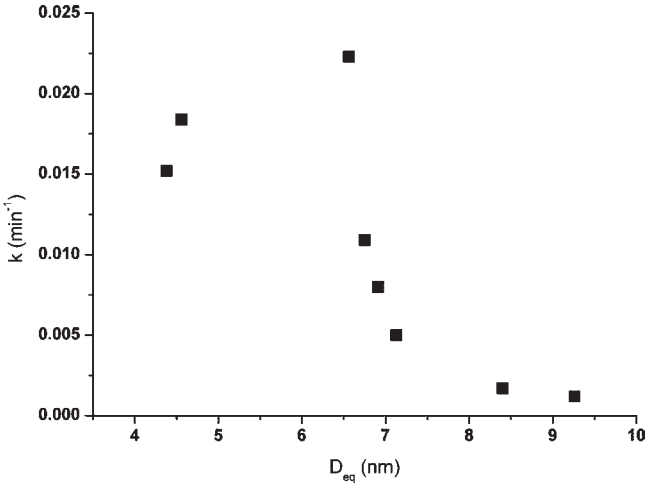

Figure 3. First-order kinetic constants (min^{-1}) vs average sample size (given as D_{eq}, the diameter of the sphere of equivalent volume) for the photochemical degradation of MB under UV−vis irradiation in the presence of identical amounts of the A1, AHW, A2, B1, B2, B3, C1, and C2 samples (left to right).

counterbalanced by O^{2-}/OH^{-} substitution. These defects, most likely distributed on the surface, have different concentration in small vs large clusters. This interpretation is indirectly supported by the Debye−Waller factors behavior, systematically showing higher values at increasing size in the *ab* plane of the anatase NCs, compensating the surplus of intensity due to an average occupancy factor that is overestimated for larger clusters.

Our ancillary characterization of the B1, B2, and B3 materials (i.e. those not requiring mechanical grinding) included: (i) determination of the N_2 sorption isotherms, showing a hysteretic effect upon cooling at about $p/p_o = 0.5$, which increases in the B1, B2, and B3 sequence and (ii) surface area measurements, with BET values all lying in the 240−270 $m^2\ g^{-1}$ range. Interestingly, the determination of the phase composition and of the *number* (bivariate) size distributions, performed by DFA analysis, allowed the independent estimation of the specific surface areas (SSA), falling in the narrow 350−392 $m^2\ g^{-1}$ range (computed taking into account both anatase and brookite NCs); this slight overestimation can be attributed to the presence of cusps and shared walls not accessible to N_2 sorption and, inter alia, confirms the versatility of the DFA method.

CONCLUSIONS

We have reported here on an innovative total scattering method, based on an original and fast way of treating the Debye equation, applied to a set of nanosized titania samples; with this approach, sizes and size distributions have been extracted from synchrotron X-ray powder diffraction data, starting from bivariate families of atomistic anatase and brookite crystal models of prismatic shape, database generation, and interatomic distances sampling. For the titania nanopowders here investigated, the method appears to be powerful enough in quantitatively rescuing small size/shape differences from apparently very similar powder diffraction patterns. Average sizes derived from mass and number distributions were employed in addressing details in the smallest and largest fractions within each sample. In addition, the analysis highlighted small differences in the NCs cell volumes and Ti ions vacancies in samples from distinct synthetic approaches.

The fairly coherent picture obtained by our DFA analysis on these materials suggests further comments: (i) even in the absence of a statistically meaningful number of samples, it was here found that both size and shape (and their distributions) affect the photochemical activity of TiO_2 NCs. Such a complex dependence was already reported for titania polymorphs; however, the quantitative evaluation of this effect has been usually associated to isotropic *average* size values only, which can be a limited way of investigating the problem; (ii) suitably tailored total scattering-based methods, such as the DFA here presented, coupled to high-quality diffraction data might allow a rigorously quantitative estimation of a number of structural and microstructural sample features which facilitates a fruitful structure−properties characterization of the nanosized materials.

ASSOCIATED CONTENT

Supporting Information. Details on the log-normal bivariate size distribution functions used in our DFA method. Tables of DFA results for crystal data and bivariate *mass* and *number* log-normal size distributions of anatase and brookite in samples A1, A2, AHW, B1, B2, B3, C1, and C2. Plots of the final best fits for all data sets, together with the 2D maps of the *mass* size distributions. This material is available free of charge via the Internet at http://pubs.acs.org.

AUTHOR INFORMATION

Corresponding Author
antonella.guagliardi@ic.cnr.it

ACKNOWLEDGMENT

Financial support by Fondazione CARIPLO, Project No. 2009-2446 is heartily acknowledged. The diffraction data of all samples were recorded at the MS4-powder beamline of the SLS synchrotron, Villigen, Switzerland. We thank the reviewers for valuable comments.

REFERENCES

(1) See, for example, the very recent papers from markedly different fields of interest: Szeifert, J. M.; Feckl, J. M.; Fattakhova-Rohlfing, D.; Liu, Y.; Kalousek, V.; Rathousky, J.; Bein, T. *J. Am. Chem. Soc.* **2010**, *132*, 12605. Woolerton, T. W.; Sheard, S.; Reisner, E.; Pierce, E.; Ragsdale, S. W.; Armstrong, F. A. *J. Am. Chem. Soc.* **2010**, *132*, 2132. Jankovic, I. A.; Saponjic, Z. V.; Dzunuzovic, E. S.; Nedeljkovic, J. M. *Nanosci. Res. Lett* **2010**, *5*, 81. Ugur, S. S.; Sanisik, M.; Aktas, A-H. *Nanotechnology* **2010**, *21*, 325603. Khaliq, A.; Sonawane, P. J.; Sasi, B. K.; Sahu, B. S.; Pradeep, T.; Das, S. K.; Mahapatra, N. R. *Nanotechnology* **2010**, *21*, 255704.

(2) See for example the review papers: Quinonez, C.; Vallejo, W.; Gordillo, G. *Appl. Surf. Sci.* **2010**, *256*, 4065–5071. Leung, D. Y. C.; Fu, X.; Wang, C.; Ni, M; Leung, M. K. H.; Wang, X.; Fu, X. *ChemSusChem* **2010**, *3*, 681–694. Zhang, J. L.; Wu, Y. M.; Xing, M. Y.; Leghari, S. A. K.; Sajjad, S. *Energy Environ. Sci.* **2010**, *3*, 715–726. Chen, X. *Chin. J. Catal.* **2009**, *30*, 839–851. Hashimoto, K.; Irie, H.; Fujishima, A. *AAPPS Bull.* **2007**, *17*, 12–28.

(3) Anatase crystallizes in the tetragonal space group $I4_1/amd$; rutile in the tetragonal $P4_2/mnm$ one and brookite is orthorhombic, *Pbca*. Structural data from ICSD #9852 (Anatase) and ICSD #36408 (Brookite).

(4) Linsebiegler, A. L.; Lu, G.; Yates, J. T., Jr. *Chem. Rev.* **1995**, *95*, 735–758.

(5) Thompson, T. L.; Yates, J. T. *Chem. Rev.* **2006**, *106*, 4428–4453.

(6) Grey, I. E.; Wilson, N. C. *J. Solid State Chem.* **2007**, *180*, 670–678.

(7) Luca, V. *J. Phys. Chem. C* **2009**, *113*, 6367–6380.
(8) Wunderlich, W.; Miao, L.; Tanemura, M.; Tanemura, S.; Jin, P.; Kaneko, K.; Terai, A.; Nabatova-Gabin, N. *Int. J. Nanosci.* **2004**, *3*, 439–445.
(9) Li, W.; Liu, C.; Zhou, Y.; Bai, Y.; Feng, X.; Yang, Z.; Lu, L.; Lu, X.; Chan, K. Y. *J. Phys. Chem.* **2008**, *112*, 20538–20545.
(10) Borse, P. H.; Kankate, L. S.; Dassenoy, F.; Vogel, W; Urban, J.; Kulkarni, S. K. *J. Mater. Sci.* **2002**, *13*, 553–559. Matej, Z.; Kužel, R.; Nichtová, L. *Powder Diffr.* **2010**, *25*, 125–131.
(11) Scherrer, P. *Gött. Nachr. Gesell.* **1918**, *2*, 98.
(12) Egami, T., Billinge, S. J. L., Eds. *Underneath the Bragg Peaks: Structural Analysis of Complex Materials*; Elsevier: Amsterdam, 2003.
(13) Cervellino, A.; Guagliardi, A. In *Diffraction at the Nanoscale: Nanocrystals, Defective and Amorphous Materials*; Masciocchi, N., Guagliardi, A., Eds.; Insubria University Press: Varese, Italy, 2010.
(14) Cervellino, A.; Giannini, C.; Guagliardi, A. *J. Appl. Crystallogr.* **2003**, *36*, 1148–1158.
(15) Debye, P. *Ann. Phys.* **1915**, *46*, 809–823.
(16) (a) Grover, R. F.; McKenzie, D. R. *Acta Crystallogr.* **2001**, *A57*, 739–747. (b) Cervellino, A.; Giannini, C.; Guagliardi, A. *J. Comput. Chem.* **2006**, *27*, 995–1008.
(17) Cervellino, A.; Giannini, C.; Guagliardi, A.; Zanchet, D. *Eur. Phys. J. B* **2004**, *41*, 485–493. Gálvez, N.; Valero, E.; Domínguez-Vera, J. M.; Masciocchi, N.; Guagliardi, A.; Clemente-León, M.; Coronado, E. *Nanotechnology* **2010**, *21*, 274017–274022.
(18) Cozzoli, P. D.; Snoeck, E.; Garcia, M. A.; Giannini, C.; Guagliardi, A.; Cervellino, A.; Gozzo, F.; Hernando, A.; Achterhold, K.; Ciobanu, N.; Parak, F. G.; Cingolani, R.; Manna, L. *Nano Lett.* **2006**, *6*, 1966–1972. Cademartiri, L.; Montanari, E.; Calestani, G.; Migliori, A.; Guagliardi, A.; Ozin, G. A. *J. Am. Chem. Soc.* **2006**, *128*, 10337–10346.
(19) Guagliardi, A.; Cedola, A.; Giannini, C.; Ladisa, M; Cervellino, A.; Sorrentino, A.; Lagomarsino, S.; Cancedda, R.; Mastrogiacomo, M. *Biomaterials* **2010**, *32*, 8289–8298.
(20) Dastjerdi, R.; Montazer, M. *Colloids Surf., B* **2010**, *79*, 5–18.
(21) As in: Strini, A.; Cassese, S.; Schiavi., L. *Appl. Catal., B* **2005**, *61*, 90–97.
(22) Sampson, P. D.; Siegel, A. F. *J. Am. Stat. Assoc.* **1985**, *80*, 910–914.
(23) Cervellino, A.; Giannini, C.; Guagliardi, A. *J. Appl. Crystallogr.* **2010**, *43*, 1543; see also: www.sourceforge.net/projects/debussy/.
(24) See for example the detailed 3D-shape reconstruction of anatase nanocrystals from HRTEM images reported in: Feldhoff, A.; Mendive, C.; Bredow, T., Bahnemann, D. *ChemPhysChem* **2007**, *8*, 805.
(25) By the simplex method: Nelder, J. A.; Mead, R. *Comput. J.* **1965**, *27*, 308–313.
(26) Correlation coefficients for A- and C-types samples lie in the 0.15−0.50 range, with the smallest values found in the largest samples of each group.
(27) Kandiel, T. A.; Feldhoff, A.; Robben, L.; Dillert, R.; Bahnemann, D. W. *Chem. Mater.* **2010**, *22*, 2050–2060.
(28) The number distribution gives the fraction of the total number of NCs possessing a given size. The mass distribution gives the fraction of the total mass of NCs possessing a given size.
(29) Only the average value based on the NCs *mass* distribution (and not on the *number* distribution) can be compared with the average crystal sizes obtained from Rietveld-like methods.